# Hydraulic fracturing-induced seismicity: an overview of recent observations and implications on development

**Adam Baig[1*] and Ted Urbancic[1] demonstrate that many instruments are insufficient to characterize induced seismicity associated with hydraulic fracturing and that more realistic target magnitudes are needed.**

An accurate magnitude calculation is critical to assessing the impact of hydraulic fracturing on seismic hazards as well as correctly characterizing the fractures that are activated during the stimulation. Recently, Warpinski (2013) asserted that seismicity associated with hydraulic fracturing rarely attains magnitudes above 0.5; on the other hand Holland (2011) documents hydraulic fracture-induced seismicity in the Eola field in Oklahoma reaching magnitudes of 2.8. While it can be argued that the latter dataset may be unusual, there is a fundamental difference between the datasets considered in that the former data are collected from downhole monitoring arrays utilizing 15Hz geophones, primarily tasked with the routine tasks of hydraulic fracture monitoring of delineating stimulation volumes with event locations; whereas Holland's study used USArray broadband stations with the low-frequency response necessary to accurately characterize the larger-magnitude events. Given the ubiquity of arrays of 10 Hz or 15 Hz geophone arrays for industrial monitoring of hydraulic fracturing, it is an open question whether and how frequently larger-magnitude events (>M0) are generated during these stimulations given the inadequacy of these instruments for characterizing larger-magnitude events.

In order to obtain the necessary low frequencies to accurately calculate the magnitudes of events associated with hydraulic fracturing, we have routinely begun deploying a lower-frequency sensor on or near the surface in combination with high-frequency Downhole arrays (hybrid configuration). We routinely detect events on these surface-deployed sensors, and for the amplitudes necessary to exceed noise levels at the surface these events are almost necessarily positive in magnitude. We show some of the magnitudes obtained from monitoring different shale plays across North America in Figure 1. Notably, the two datasets in the Horn River and the two in the Eagleford are relatively proximate, and we observe a very different response indicating that the occurrence of these events can be very dependent on local structures in close vicinity of the treatments. The scale of the fractures/faults associated with these higher magnitudes is typically in the tens of metres and above range, so the activation of these events in terms surface area activated potentially has very profound implications on the geomechanical behaviour of the reservoir.

We suggest that previous reports of the dearth of large magnitude (M>0) induced seismicity events associated with hydraulic fracturing have been coloured by the use of instruments insufficient to characterize these events and that regulations such as traffic light systems need more realistic target magnitudes in order to better respond to magnitudes that may be typically observed in hydraulic fractures. For example, the UK regulations of a halt of injection when an M0.5 is detected may impede the growth of industry if events of this relatively benign magnitude are regularly generated. Based on our sampling of datasets, we detect M0+ events relatively frequently.

The implications of these larger-magnitude events on the datasets recorded are very profound, not just for the reporting and mitigation of potentially felt seismicity, but also on the geomechanical description of the fracturing process in the reservoir. Lower-frequency sampling of the data enables proper characterization of the reservoir in terms of the activated fracture size scales and their associated stress releases, enabling a proper context to be put to the activation of these events.

For example, if the events are representative of stress-shedding on larger fault structures, and not necessarily representing a fluid activation, then the stress releases will generally be higher. It is well-known that only a fraction of an event's energy is radiated seismically (Aki and Richards, 2002). The energy budget of the stress-shedding events will generally devote more energy towards seismic radiation, since features optimally oriented to slip are critically stressed then the events need to devote a relatively low percentage of their energy budget towards overcoming frictional energy, dissipating as heat and coseismic deformation. Fluid-driven seismicity usually is more inefficient

[1] *ESG Solutions.*

[*] *Corresponsing author, E-mail: adam.baig@esgsolutions.com*

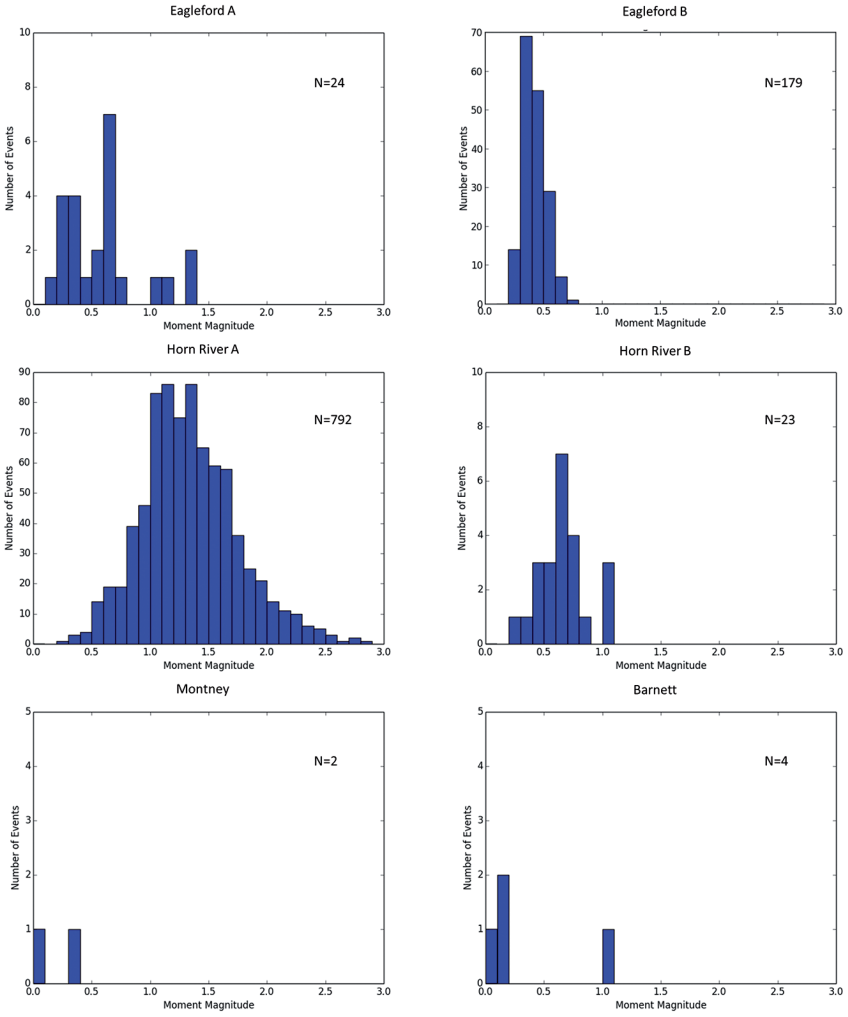


***Figure 1*** *Magnitudes histograms of M>0 events detected from surface monitoring of a number of different shale plays in North America.*

at radiating energy. We examine a case study comparing the higher-magnitude seismicity with the lower-magnitude seismicity routinely characterized by the downhole array. We examine both the stress release parameters, and the dominant mechanisms to determine if the underlying driving processes responsible for the generation of the seismicity is significantly different.

The timing of the higher-magnitude seismicity from the surface data can be related to the injection parameters to gain a better understanding of the conditions that lead to the generation of these events. Comparing the timing of the events with the pressure curves in a second case study will indicate the conditions that lead to the activation of these larger structures.

Finally, there has been considerable attention paid to the overall energy budget of the hydraulic fracturing process, and the total energy expressed as radiated seismic energy. By only relying on the downhole signals associated with the event, the total energy is generally widely underestimated. We show for the latter case study the amount of energy missed in the bandwidth outside the 15 Hz sensors can be a large fraction of the total radiated energy.

## Hybrid monitoring for full-band seismicity

The use of 10 or 15 Hz geophones in microseismic monitoring introduces limitations in what can be observed in terms of the bandwidth that can be accurately resolved. For larger-magnitude events, with significant low-frequency energy below the natural frequencies of these sensors, the signals on these sensors will be saturated, and will appear as smaller events with different corner frequencies. An example of a saturated signal is shown as the *SV* component of a waveform from a hydraulic fracture monitored from just above the treatment zone on the right of Figure 2. The low-frequency displacement spectral plateau, from which the moment magnitude is determined, is observed to have an amplitude of $6e10^{-10}$ m·s, which translates to a moment magnitude of -0.3, and an apparent corner frequency of 50 Hz. The saturation of this signal is only evident when examining the same event, as recorded on a 4.5 Hz geophone on the surface

geophone (left of Figure 2). Despite the fact that this sensor is deployed near the surface, and is much farther away from the treatment zone than the former sensor, the low-frequency amplitude is larger, at $3e10^{-9}$ m·s, translating to a magnitude of 0.7. The higher amplitude is due to this sensor being able to resolve a much lower corner frequency of 7 Hz.

Such a configuration as described above, with arrays of 15 Hz sensors deployed downhole complemented with lower-frequency sensors such as the 4.5 Hz geophone discussed in Figure 2 or force balanced accelerometers that can resolve much lower frequencies down to 0.1 Hz deployed above the reservoir, allows for larger events to be accurately characterized while still using the 15 Hz geophones near the reservoir to accurately locate the events from the recorded *P* and *S* waves. The 15 Hz sensors can generally be deployed to much lower depths since they generally have higher operating temperatures than the lower-frequency sensors, while the lower frequency sensors are deployed farther away (including close to the surface) to ensure that the observed signals are in the far field. Although geometrical spreading will attenuate the signals, these larger-magnitude events will naturally have larger amplitudes, and the detectability will be over greater distance.

An example configuration is depicted in Figure 3. In the depth view on the left, there are three sensor arrays of 15 Hz sensors comprising 24 or 36 levels. Eight stations consisting of 4.5 Hz geophones and force balance accelerometers are deployed in shallow wells to depths of 30 m.

## Case Study 1: Contrasting M>0 with M<0 events in the Horn River Basin

For the first case study that we discuss, we contrast around 800 events with M>0 in the Horn River Basin detected from the near-surface network illustrated in Figure 3 with 400 events from a stage of a hydraulic fracture completion detected with multiple downhole arrays of 15 Hz sensors.

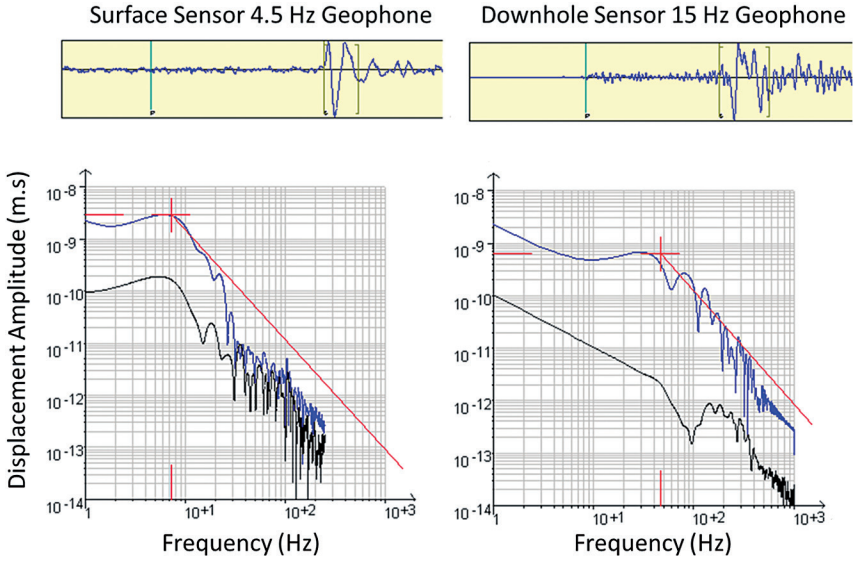


***Figure 2*** *SV Waveforms from an Mw0.7 event during a hydraulic fracture stimulation recorded from (left) a near-surface deployed 4.5 Hz geophone and (right) a downhole-deployed 15 Hz geophone. The saturated response on the 15 Hz geophone leads to a biased magnitude calculation of -Mw0.3.*

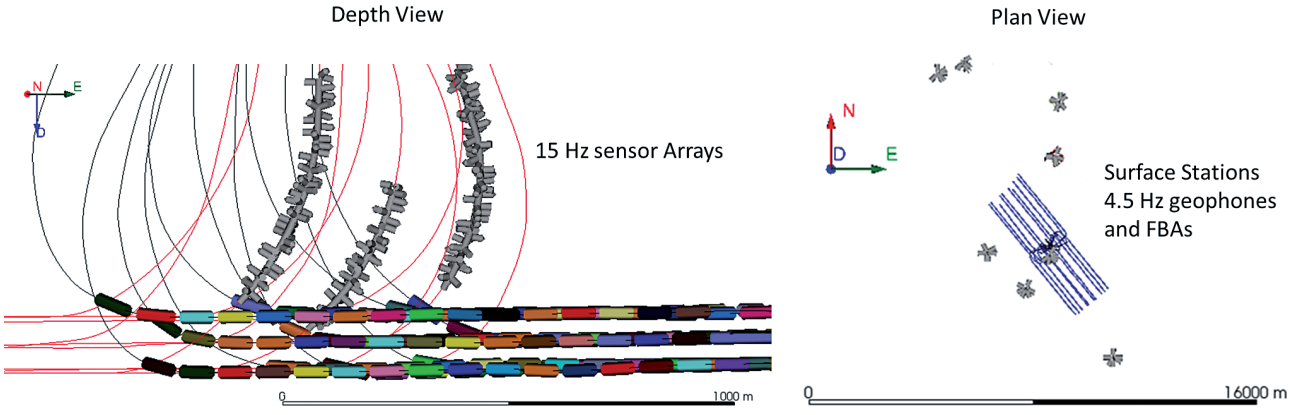


***Figure 3*** *Depth (left) and plan (right) views of a hybrid near-surface downhole network of arrays of 15 Hz geophones directly above the reservoir with near-surface stations of 4.5 Hz geophones and force-balance accelerometers (FBAs).*

The largest events detected on the near-surface network approached Mw3, and were detected on the nearest CNSN station in Fort Nelson, British Columbia, about 100 km away. For each dataset, we can calculate source parameters such as a moment magnitude and source radius from the observed corner frequencies and spectral plateaus as well as (where data quality allows) general moment tensor solutions. Therefore, we can both assess the scaling behaviour of both datasets as well as the mechanisms. Using both analyses, the proper contextualization of the larger-magnitude events can be determined through comparison of the lower-magnitude seismicity associated with the downhole arrays representing the steady growth of the hydraulic fractures from the perforations.

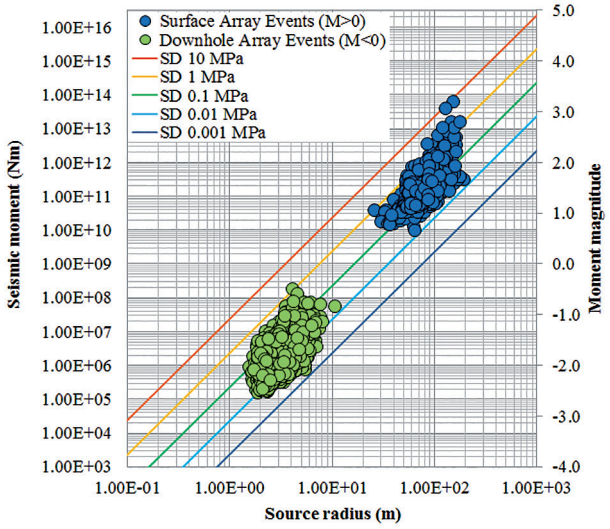


***Figure 4*** *Source radius versus seismic moment (and therefore moment magnitude) along with lines of equal static stress drop show the scaling relationships for the larger-magnitude events detected with the near-surface array (in blue) and smaller magnitude downhole recorded dataset (in green).*

We show the difference in scaling between the M>0 and M<0 datasets by plotting moment versus source radius against lines of constant stress drop in Figure 4. Each of the large- and small-magnitude datasets appears to be self-similar within their own scatter, since they tend to scatter along lines of constant stress drop. However, the stress drops for the larger-magnitude seismicity appears to be on average about one order of magnitude higher than the lower-magnitude seismicity. The suggestion of this analysis suggests that the higher-magnitude seismicity is responding to a more stress-driven process responsible for the larger-magnitude events than the smaller-magnitude events with on average smaller stress releases, more typical of fluid-driven processes.

To further contextualize these data, we compare the general moment tensor solutions for the M>0 and M<0 datasets, to illustrate systematic differences in the source types (Hudson et al., 1989) for these events in Figure 5. Although both datasets show significant non-double-couple components, both generally characterized by mixed-mode shear-tensile failures, the larger-magnitude events show a more shear-dominant signature than the lower-magnitude events with a stronger tensile opening component overall. Further analysis of the mechanisms reveals the dominant fracture planes for the two families of events. By applying the analyses described by Baig and Urbancic (2010) to assign an orientation to different modes of failures, the differences in the dominant fracture planes can be visualized through rosette diagrams, as shown in Figure 6 with the natural fractures of the area (Reine and Dunphy, 2011) displayed for comparison. For reference, the direction of SHmax in the area is roughly NE-SW. The two datasets show significantly different distributions, with the larger-magnitude dataset indicating a distribution that is optimally oriented to slip in

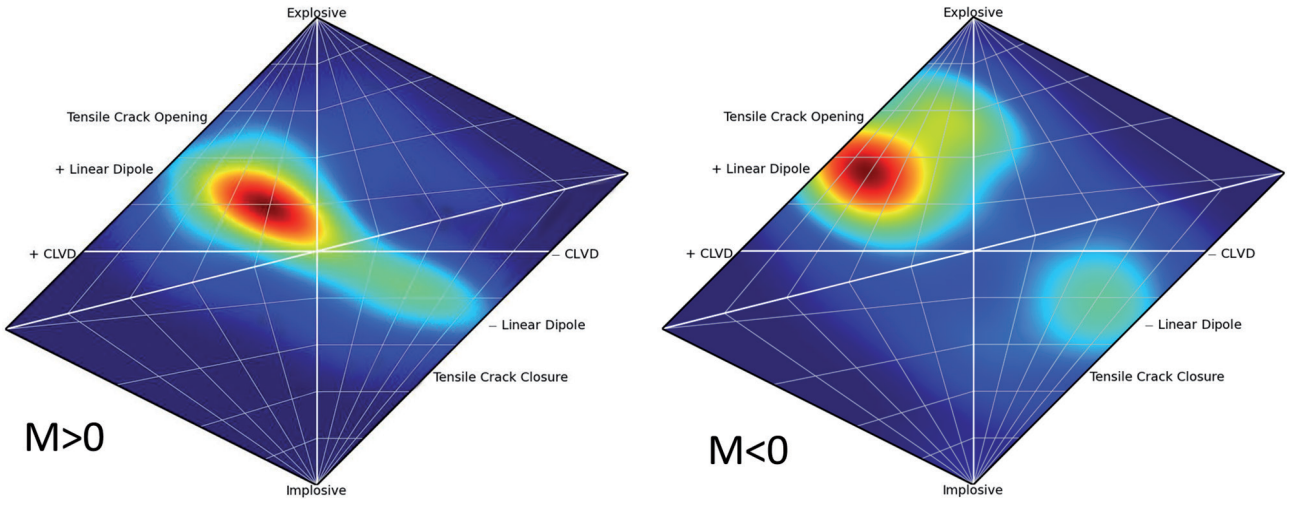


***Figure 5*** *Source-type plots for both the surface recorded Mw>0 and downhole Mw<0 datasets.*

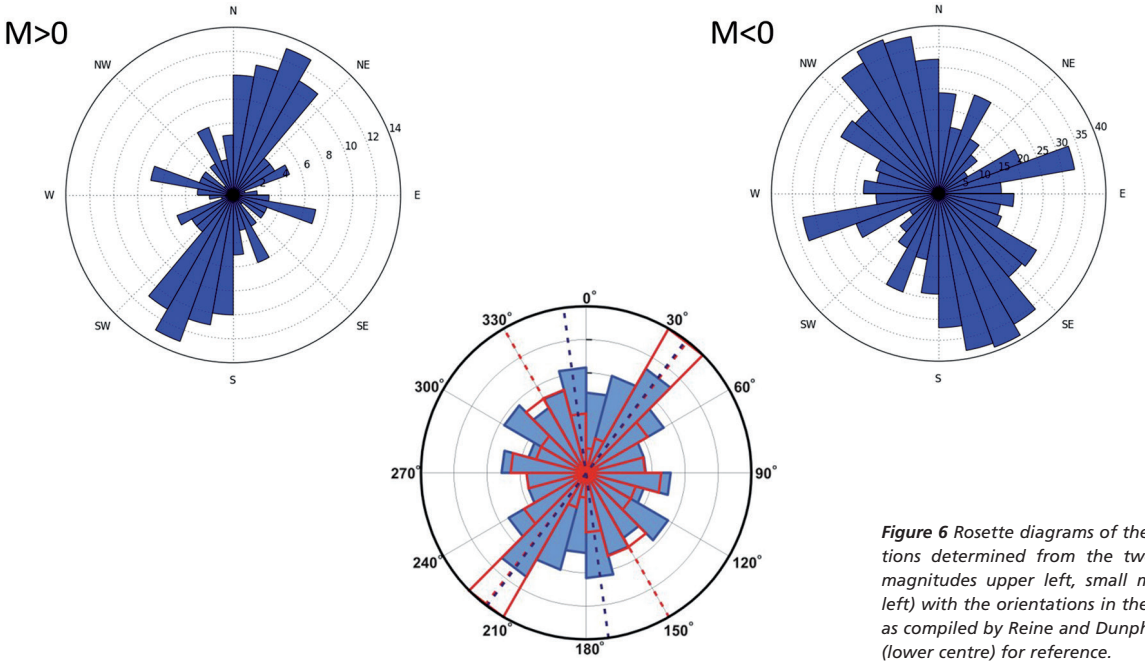


***Figure 6*** *Rosette diagrams of the fracture orientations determined from the two datasets (large magnitudes upper left, small magnitudes upper left) with the orientations in the Horn River Basin as compiled by Reine and Dunphy (2011) included (lower centre) for reference.*

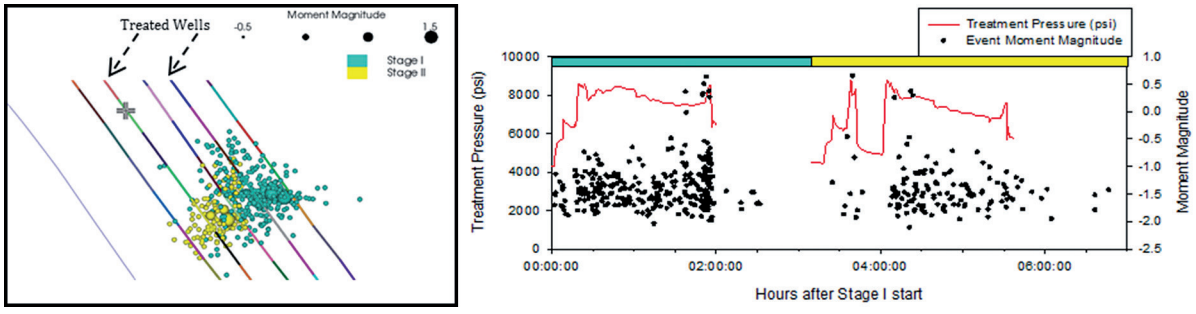


***Figure 7*** *Two stages where larger events during a zipper frac completion in the Eagleford are shown in plan view (left) and against the treatment pressure with magnitude (right) against time.*

the stress regime of the Horn River Basin, and the smaller-magnitude dataset showing very different orientations.

Summarizing the comparisons of these two datasets, the larger-magnitude seismicity is characterized by more shear-driven failures with higher stress drops on fractures that are optimally oriented with respect to the regional stress regime in the Horn River Basin. The lower-magnitude seismicity follows lower stress drops on fractures not optimally oriented to the regional stress indicating more tensile components. The differences in these results suggest that for these datasets the larger magnitudes are occurring due to stress perturbations from the injection acting on optimally oriented faults that are critically stressed, whereas the lower-magnitude seismicity is a more fluid-driven process responding to perturbations in the stress regime. Features activated by the lower-magnitude events are more likely activating joint sets with fracture lengths in the order of a few to a few tens of metres in radius, whereas the larger magnitudes are activating faults with features of radii on the order of a few hundred metres. Based on these observations, we suggest that there is a sufficient stress transfer and stress build up resulting from the smaller events to allow for pre-existing faults to slip in shear. The presence of these faults that can be activated by the stress-shedding effects during hydraulic fracture treatments, can have profound effects on the understanding of the fracture propagation in the reservoir, and create potential pathways that can lead to either enhanced or ineffective stimulations.

## Case Study 2: Larger-magnitude events in the context of injection programmes

We consider a second case study in the Eagleford where a zipper-frac completion was monitored from a single vertical array of 15 Hz geophones and a near-surface network of 4.5 Hz geophones and force-balance accelerometers. A number of larger-magnitude events were observed in this dataset, and we focus on two stages (depicted on the left of Figure 7 in plan view). All of the larger events, detected and characterized by the near-surface network, occur with

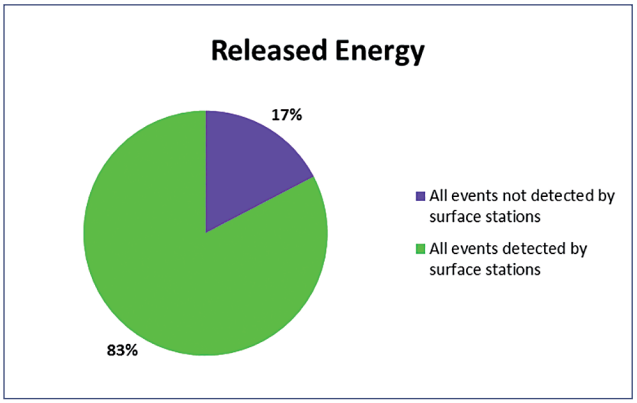


***Figure 8*** *Radiated seismic energy from the 28 events recorded on the near-surface stations comprise more than 80% of total energy recorded during the completion. The balance of the 4500 events only total up to less than 20% of the total detected radiated energy.*

the highest treatment pressures (right of Figure 7). The concurrence of the high pressures with the activations of these events, representing features up to 100 m in source radius, indicates a very close relationship between the injections and these failures. Without the lower-frequency signals from the near-surface network, the larger magnitudes would not stand out from the main distributions, and the suggestion of larger-magnitude events tied to the injection would not be evident.

Furthermore, for this dataset, we show that the contribution of the surface-detected events to the overall total radiated seismic energy is quite marked. In Figure 8 we show that despite the fact that only 28 events were detected over the whole completion from the surface network, these data comprise 83% of the energy release; the balance of the 4500 events seen on the downhole network pale in comparison in terms of energy release, only totally 17% of the energy release. The larger-magnitude seismicity only liberates about 4% more surface area than the other events, but during the stages where these events are more frequent, this percentage can jump to about 27% extra surface area.

## Conclusions

Near-surface arrays of lower-frequency sensors combined with downhole arrays of 15 Hz geophones allows for characterization of the full band of seismicity generated during hydraulic fracturing. Detecting larger-magnitude events using these hybrid arrays suggests that previous claims of the dearth of such events during hydraulic fracturing may have failed to account for the lack of low-frequency response from the 15 Hz geophones. Although larger events may be more ubiquitous than previously claimed, the implications for seismic hazard are more modest than what these events mean in terms of the response of the reservoir to the treatment. In the first case study, contrasting larger- and smaller-magnitude (>M0 and <M0, respectively) events shows that the events are clearly responding to different stress processes. Larger magnitude events are more shear-driven, likely to be representing stress transfer on to optimally oriented features whereas the smaller magnitude events show a stronger fluid-driven signature. For the second case study, the occurrence of the larger-magnitude events during the highest treatment pressures suggests a strong connection to the injection process. Finally, failure to account for the low-frequency response of the event can result in significant underestimation of the overall radiated energy for the seismicity associated with the fracturing.

## References

Aki, K. and Richards, P.G. [2002] *Quantitative Seismology: Theory and Methods*. University Science Books, ISBN 978-1-891389-63–4.

Baig, A.M. and Urbancic, T.I. [2010] Microseismic moment tensors: A path to understanding frac growth. *The Leading Edge*, **29**, 320–324.

Holland, A. [2012] Examination of possibly induced seismicity from hydraulic fracturing in the Eola Field, Garvin County, Oklahoma. *Oklahoma Geological Survey, Oklahoma*, open-file report., OF1-2011, 28.

Hudson, J.A., Pearce, R.G. and Rogers, R.M. [1989] Source-type plot for inversion of the moment tensor, *Journal of Geophysical Research*, **94**, 765–774.

Reine, C.A. and Dunphy, R.B. [2011] Weighing in on the Seismic Scale: The use of Seismic Fault Measurements for Constructing Discrete Fracture Networks in the Horn River Basin. *Recovery – 2011 CSPG CSEG CWLS Convention*, Abstracts.

Warpinski, N.R. [2014] A Review of Hydraulic-Fracture Induced Microseismicity. *48th meeting of American Rock Mechanics Associate*, Abstracts.